PHYSICAL REVIEW E VOLUME 52, NUMBER 2 AUGUST 1995

Computer simulation of the rheology of grafted chains under shear

G. H. Peters

Chemistry Department III, H.C. Ørsted Institutet, University of Copenhagen, Universitetsparken 5, DK-2100 Copenhagen Ø, Denmark and Novo-Nordisk A/S, Novo Allé 1, DK-2880 Bagsvaerd, Denmark

D. J. Tildesley

Chemistry Department, University of Southampton, Southampton SO9 5NH, United Kingdom

(Received 14 November 1994)

We report nonequilibrium molecular dynamics simulations of grafted chains surrounded by solvent molecules and sheared between two atomic walls. Each wall is covered by a layer of amphiphilic molecules 20 units long. The chains are firmly bound at their ends to the wall at a surface coverage of 33%. The particles interact through the Weeks-Chandler-Andersen repulsive potential. Bond interactions and the stiffness of the chains are modeled using harmonic potentials. The heat produced by shearing is removed from the system by conduction through the boundaries, which leads to characteristic gradients in temperature, density, and shear rate. At low shear rates, these effects are small, but structural reordering of the solvent molecules and chains is observed. Solvent molecules are expelled from the chain region close to the boundary wall during shearing. Decreasing the flexibility of the amphiphilic molecules creates a more dramatic response to the imposed shear field, resulting in a larger chain tilt and fewer solvent molecules close to the wall.

PACS number(s): 36.20.Fz

I. INTRODUCTION

Adsorption of flexible long chain polymers at a solid liquid interface occurs in a wide range of important technological problems, such as enhanced oil recovery, lubrication, filtration, and in the production of miniature motors and aerospace devices. Many modern instruments require smooth, low-friction surfaces to reduce wear and increase equipment lifetime. Modeling the boundary lubrication process requires a detailed understanding of the properties of liquids in a confined geometry and an investigation of the effect of grafted amphiphiles on the rheology of the system. Friction and rheological properties of molecularly thin films has been extensively studied by experiment [1–8], theory [9–11], and computer simulation [12–16].

These results have provided a preliminary understanding of the friction occurring when two smooth solid surfaces separated by a thin liquid film slide past one another. For pores containing pure solvent the trapped liquid film becomes progressively thinner and its physical properties change from those of the bulk fluid to those of a thin solid. At high loads and low shear rates, many molecularly thin films show a complex behavior involving liquid-to-solid phase transitions, the appearance of new liquid-crystalline phases, and epitaxially induced long-range ordering [1,5]. The process is further complicated by the adsorption of lubricants such as graphite, inorganic compounds, and amphiphilic molecules at a solid boundary.

Macroscopically, friction is usually accompanied by wear and conductive heat flow and amphiphiles are used to reduce wear. Many studies have investigated the mechanism by which the system dissipates energy using first principles calculations [17,18] based on *ab initio* total energy calculations of moving two layers past each other or molecular dynamics simulations [19,21]. Harris *et al.* [19,20] studied the friction of two sliding diamond interfaces coated with chemically bonded short alkanes. Much longer hydrocarbons were used by Glosli and McClelland [21] to investigate the friction and energy dissipation between ordered organic monolayers. These studies were performed without considering the solvent, which in many applications may play an important role. Therefore, we are primarily interested in simulating the lubrication in a wet environment, i.e., in the presence of solvent molecules.

Most of the computational studies were performed using the traditional atomic-scale modeling of atoms and molecules. However, many physical properties have different characteristic length scales and could be described by a more coarse-grained model and meso-scale computer modeling [22]. This coarse graining can significantly reduce the computational burden, and provides an avenue to simulate and study collective and cooperative behavior of a larger number of interacting molecules, such as phase separation, formation of micelles, and viscoelasticity. Meso-scale modeling has already been successfully applied in theoretical studies [23,24], Monte Carlo [25–31], and molecular dynamics simulations [32–36] of polymers.

In our study of shear induced flow, we have applied meso-scale modeling to examine the effect of coating two opposite walls with amphiphilic molecules on the fluid structure, friction, and viscosity of a pure solvent. This is a typical industrial problem encountered in fabric softening [37], where amphiphiles (surfactants) are added during the washing to enhance the condition of the fabric

1063-651X/95/52(2)/1882(9)/$06.00 ©1995 The American Physical Society

and the conditioning of hair before wet combing. The physical properties of such a complex system depend on many parameters such as wall separation, surface coverage, and chain length to mention only a few. We have chosen a small set of parameters to capture the main features of the shearing process. In particular, we would like to address the following fundamental questions:

(1) How do grafted amphiphiles change the viscosity profile?

(2) Is the stress (friction) profile constant across the shear field?

(3) How does the solvent adapt to the amphiphiles?

(4) Are solvent molecules trapped in the organic layer?

(5) How does flexibility of the chains influence the rheological properties?

We have decided to simulate three different systems at relatively low coverage, where we still expect to obtain reliable structural and rheological information. These systems are the pure Lennard-Jones fluid and surfactants of different flexibility immersed in solvent and chemically bonded to the wall. Each system was studied at seven different shear rates.

We have chosen to compute the viscosity by using a nonequilibrium method rather than the zero-shear Green-Kubo technique [10]. We are interested in how the shearing changes the structural characteristics of the amphiphilic layer. Unfortunately, we have to use a relatively high shear rate compared to experiment. Sliding velocities used in surface force apparatus can be as high as several tens of μm/s. Typical shear rates in these experiments are between 10^{-7} and 10^{-4} ns^{-1} [5]. Sliding velocities of the order of 0.1 mm/s are applied in determining friction and shear behavior of fabric softeners [37]. Assuming a chain of block polymers where each unit is of size 100 Å with an average mass of 50 000 g/mol, our sliding velocities are of the order of 1 m/s. This does not seem unreasonable for problems such as sliding fabrics or hair fibers.

The paper is organized as follows. In Sec. II we describe the potential model and simulation details used in our shearing experiment. Section III contains a discussion of our results obtained for the pure Lennard-Jones fluid, amphiphilic molecules immersed in the solvent and tethered to the walls, and for a second amphiphile with stiffer chain. Finally, we conclude by summarizing the changes of the rheological properties observed due to the addition of amphiphilic molecules and the effect of increasing chain stiffness.

II. MODEL AND SIMULATION

The model used in our computational study and displayed in Fig. 1 is composed of solvent molecules, amphiphilic chains, and two atomic boundary walls. The interaction between all particles is described by a shifted and truncated Lennard-Jones potential known as the repulsive Weeks-Chandler-Andersen (WCA) potential [38] and given by

$$U_{\mathrm{LJ}}=4\epsilon\left[\left[\frac{\sigma}{r}\right]^{12}-\left[\frac{\sigma}{r}\right]^{6}\right]+\epsilon,\quad r\leq 2^{1/6}\ , \tag{1}$$

$$U_{\mathrm{LJ}}=0,\quad r>2^{1/6}\ , \tag{2}$$

where σ and ϵ are the collision diameter and the well depth of the potential, respectively. This potential is truncated and shifted at the minimum of the full Lennard-Jones potential and only includes repulsive contributions. Additional attractive potentials are required for the bead-bead interaction in the chains and to keep certain particles in the crystal lattice that forms the wall. The intramolecular bead interactions are modeled by the bead spring potential [32], where beads are connected by an anharmonic spring [33–35] of the form

$$U_c=-\tfrac{1}{2}k_cR_0^2\ln\left[1-\left[\frac{r}{R_0}\right]^2\right],\quad r\leq R_0\ , \tag{3}$$

$$U_c=\infty,\quad r>R_0\ . \tag{4}$$

The adopted values for k_c and R_0 are $30\epsilon/\sigma^2$ and 1.5σ and are taken from Ref. [35].

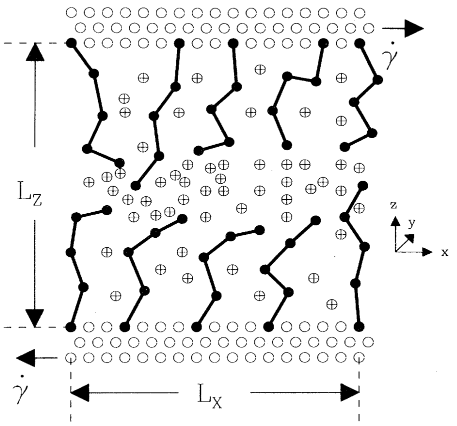

FIG. 1. Schematic representation of the simulation cell. Open circles, circles marked with a cross, and filled circles represent boundary, fluid, and chain particles. $\dot\gamma$ indicates the direction of the displacement of the wall particles to impose a shear field on the fluid.

The stiffness of the chains is controlled by including one additional harmonic potential acting between beads i and $i+2$:

$$U_{bd,ik}=\tfrac{1}{2}k_{ik}(|\vec r_{ik}-\vec r_{\mathrm{eq},ik}|)^2,\quad k=i+2 \tag{5}$$

with $\vec r_{\mathrm{eq},ik}=1.9216\sigma$, which is twice the distance of the location of the minimum of the potential given by Eqs. (1)–(4). The force constant k_{ik} is equal to k_c defined above. Two sets of simulations were performed using ($k_{ik}=0$) and ($k_{ik}=30$). Henceforth, these two sets of parameters are referred to as LJ+C (Lennard-Jones plus chains) and LJ+SC (Lennard-Jones plus stiff chains).

The wall atoms are attached to their initial lattice points, $\mathbf{r}_{\mathrm{eg},i}$, by a harmonic potential

$$U_{bd,w}=\tfrac{1}{2}k_w(|\mathbf{r}_i-\mathbf{r}_{\mathrm{eq},i}|)^2\ . \tag{6}$$

The force constant $k_w=72\epsilon/(2^{1/3}\sigma^2)$ is equal to the numerical value of the second derivative of the full Lennard-Jones potential determined at the minimum of the potential [13]. This yields a harmonic potential well, which is comparable to the full LJ potential [14]. It is sufficiently deep to prevent the wall atoms from moving from their equilibrium positions, and at the same time, provides a thermal bath for removing heat from the system and preventing solvent molecules from entering the wall region. Each wall contains 306 particles arranged in three hexagonally close packed layers. In view of the short range nature of the WCA potential, the boundary thickness is sufficient that solvent particles which are trapped close to the walls do not experience a direct force from the outermost layer.

The nonequilibrium molecular dynamics (NEMD) simulations [39–41] were performed in an orthorhombic cell with periodic boundary conditions applied in the x and y directions. Along the z direction, the fluid is bound by the two walls. The cell dimensions L are in reduced units: $L_x=17.0$, $L_y=5.83$, and $L_z=33.80$. The initial configuration, shown schematically in Fig. 1, was generated by randomly tethering amphiphilic molecules of chain length 30 beads to each wall corresponding to a coverage of 33% and randomly placing solvent molecules in the simulation cell resulting in a total density of $\rho=N/V=0.825$. N is the total number of particles in the cell of volume V. At this statepoint, chains attached to opposing walls are separated by a solvent region, which in the most extended conformation of the chains is of thickness of $(1-2)\sigma$.

The equations of motion were integrated using a leapfrog algorithm [42] with a time step of $\Delta t=0.025\tau$, where $\tau=(\epsilon/m\sigma^2)^{-1/2}$ is the usual Lennard-Jones time unit. The temperature of each wall was controlled with a Nosé-Hoover thermostat [43] and maintained at an average temperature of $T^*=k_BT/\epsilon=2.083$, where k_B is Boltzmann's constant. Simulations were performed at a series of low shear rates, $\dot{\gamma}^*=\dot{\gamma}\sqrt{(m\sigma^2/\epsilon)}$, ranging from 0 to 0.101. Shear flow was induced by using sliding boundaries. This technique was first used by Ashurst and Hoover [44], and shear is induced by translating the lattice sites associated with walls atoms in the top and bottom wall in opposite directions by a distance Δx. The magnitude of the displacement is determined by the applied shear rate and given by

$$\Delta x=\pm\tfrac{1}{2}\dot{\gamma}L_z\Delta t\ . \tag{7}$$

As shown in Fig. 1, L_z is defined as the distance between anchoring lattice points of boundary layers nearest the fluid [13]. This technique is comparable to the homogeneous-shear method [45–47], and for simple homogeneous liquids, converges to the Green-Kubo result at zero-shear rate [10].

A typical run for a given shear rate consisted of 50 000 NEMD steps, which were discarded to account for the equilibration as the system adjusted to the new shear rate, and a sampling phase of 200 000 NEMD steps, where thermodynamic and structural quantities were collected. The equilibrated configuration was then used as the starting configuration for the next higher shear rate. Again 50 000 NEMD steps were applied for equilibration and 200 000 NEMD steps were applied for sampling. This procedure was repeated sequentially up to the highest shear rate.

III. RESULTS AND DISCUSSIONS

We have investigated three different model systems to study the effect of amphiphilic molecules immersed in solvent molecules on the shear viscosity and stress. The first model consists of a pure Lennard-Jones fluid, whereas in the second model, amphiphilic molecules were tethered to the wall and surrounded by solvent molecules. The latter we will refer to as LJ+C (Lennard-Jones plus chains). In third model, we increased the stiffness of the chains by including an additional harmonic potential [Eq. (5)]. This model we will refer to as LJ+SC (Lennard-Jones plus stiff chains). For comparison, we begin by presenting the results of the LJ fluid, which has been investigated earlier [13] at a relatively high shear rate. The lowest shear rate applied in this study was two orders of magnitude lower than the one reported in Ref. [13], and as discussed later, represents the lowest shear rate that can be effectively used in the simulations, because the signal to noise ratio became too high at lower shear. The shear field imposed by sliding the wall particles results in a gradual increase in temperature. To monitor the temperature evolution throughout the system, we calculated the average slab temperature

$$T_z(z_n)=\left\langle \frac{\sum_{i=1}^{N} H_n(z_i)m_i[v_{z,i}-u_z(z_n)]^2}{k_B\sum_{i=1}^{N} H_n(z_i)} \right\rangle , \tag{8}$$

where $\langle\ \rangle$ denotes a time average. m_i is the mass of particle i located in the slab n, and $H_n(z_i(t))$ is a function of the form

$$H_n(z_i)=1 \quad \text{for } z_n-\Delta z/2<z_i<z_n+\Delta z/2\ , \tag{9}$$

$$H_n(z_i)=0 \quad \text{otherwise}\ . \tag{10}$$

$u_z(z_n,t)$ in Eq. (8) is the instantaneous slab velocity in the z directions computed as $\sum_{i=1}^{N}H_n[z_i(t)]v_{z,i}(t)/N_n$, where $N_n=\sum_{i=1}^{N}H_n(z_i(t))$. Figure 2 shows the temperature profile at low, medium, and high shear rates [curves (A) to (C)]. At low shear rate, the conduction across the boundary is sufficiently fast that the fluid maintains the same temperature as the thermostatted atoms in the walls. Only at higher shear rate does the typical parabolic temperature profile develop due to the accumulation of heat in the fluid. The kink observed at the lower wall (small z) is due to the slab width used for sampling, which was $\Delta z=1.2\sigma$. Given the position of the origin at the wall-fluid interface there are not enough particles in this particular slab to obtain an accurate estimate of the temperature. The choice of Δz was guided by a recent study [13], which showed that the error in $T_z(z_n)$ is proportional to $(\Delta z)^2$ and increases when the number of particles in the slab is much less than approximately 100.

There are two important thermodynamic quantities which are of interest. First, the shear stress (negative of the appropriate off-diagonal pressure tensor component

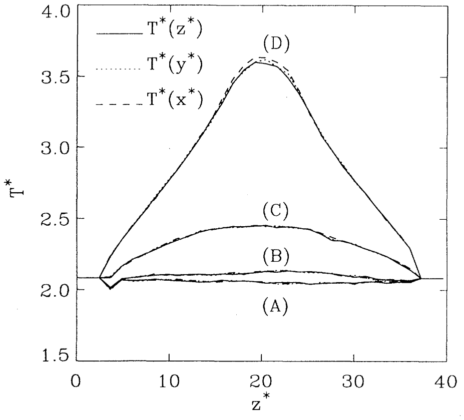

FIG. 2. Temperature profiles at distinct shear rates computed during the simulation of the LJ fluid and amphiphilic molecules immersed in solvent (LJ+SC). (*A*) LJ fluid, $\dot{\gamma}^*=0.0$; (*B*) LJ fluid, $\dot{\gamma}^*=0.040$; (*C*) LJ fluid, $\dot{\gamma}^*=0.101$; and (*D*) LJ+SC, $\dot{\gamma}^*=0.101$. Quantities are given in reduced units, where $x^*=x/\sigma$, $y^*=y/\sigma$, $z^*=z/\sigma$, $T^*=k_BT/\epsilon$, and $\dot{\gamma}^*=\dot{\gamma}\sqrt{(m\sigma^2/\epsilon)}$.

[48]), where $-P_{xz}/P_{zz}$ is the friction coefficient between the walls; and second, the viscosity, which is defined as

$$\eta(z)=\frac{\langle -P_{xz}(z)\rangle}{\dot{\gamma}(z)}\ , \tag{11}$$

where the instantaneous shear rate $\dot{\gamma}(z)$ is given by $du_x(z)/dz$. To determine the stress, we used the Irving-Kirkwood definition of the pressure tensor [49,50]:

$$\mathsf{P}(z)=\rho(z)k_BT\mathsf{I}-\frac{1}{L_xL_y}\left\langle\sum_{i<j}\frac{\mathbf{r}_{ij}\mathbf{r}_{ij}}{|\mathbf{r}_{ij}|}\frac{dU}{dr_{ij}}\frac{1}{|z_{ij}|}\times\theta\left[\frac{z-z_i}{z_{ij}}\right]\theta\left[\frac{z_j-z}{z_{ij}}\right]\right\rangle . \tag{12}$$

I is the unit tensor, $\langle\ \rangle$ denotes a configurational average, and θ is a unit step function, which is 1 for every positive value of its argument and 0 otherwise. In the simulations, the kinetic contribution to the pressure tensor was calculated from the momentum flux [51], which was sampled at each time step, whereas the configurational contribution was computed in intervals of ten time steps. Figures 3 and 4 show the normal and off-diagonal components of the pressure tensor. $P_N(z)=P_{zz}(z)$, as required by mechanical stability [52], is constant over the fluid region. Oscillations observed close to the wall are due to density fluctuations. $P_{xz}(z)$ shown in Fig. 4 becomes more negative with increasing shear rates. We note that even at the highest shear studied, the pressure component remains constant between the two boundaries (an indication that at these shear rates, the stress could also be calculated simply by the interactions between fluid and wall particle interactions confirming the method used by Liem, Brown, and Clarke [13]). Structural ordering in the fluid was determined from the instantaneous number density in the slab n:

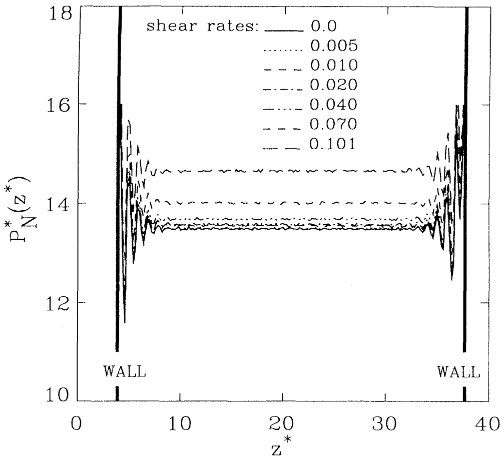

FIG. 3. Normal pressure tensor component profiles, $P_N^*(z^*)=P_N^*\sigma^3/\epsilon(z/\sigma)$, at different shear rates computed during the simulation of the LJ fluid. Shear rates are given in reduced units. See Fig. 2 caption for more details.

$$\rho(z_n)=\left\langle\frac{1}{L_xL_y\Delta z}\sum_{i=1}^{N}H_n(z_i)\right\rangle . \tag{13}$$

Histograms for the solvent particles and for all particles in the system were updated every ten time steps. Figures 5(a)–5(d) show the profiles at three different shear rates for the two systems LJ+C and LJ+SC. Even at the lowest shear rate, the solvent density at the wall is depleted and particles are pushed towards the middle of the simulation cell; see Figs. 5(a) and 5(b). Note that the solvent molecules are essentially moved from the wall to the ends of the chains. Surprisingly, within the statistical error, the profiles do not change further as the shear rate is increased from 0.005 to 0.040. At $\dot{\gamma}^*=0.101$, the density in the fluid region is slightly lower and the density close to the wall increases. In the case of the LJ+SC system, as seen in Figs. 5(c) and 5(d), the effect of removing the solvent molecules from the wall is more pronounced, and

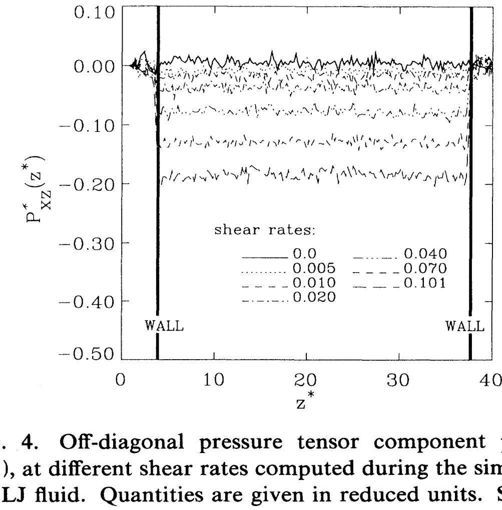

FIG. 4. Off-diagonal pressure tensor component profiles, $P_{xz}^*(z^*)$, at different shear rates computed during the simulation of the LJ fluid. Quantities are given in reduced units. See captions for Figs. 2 and 3 for more details.

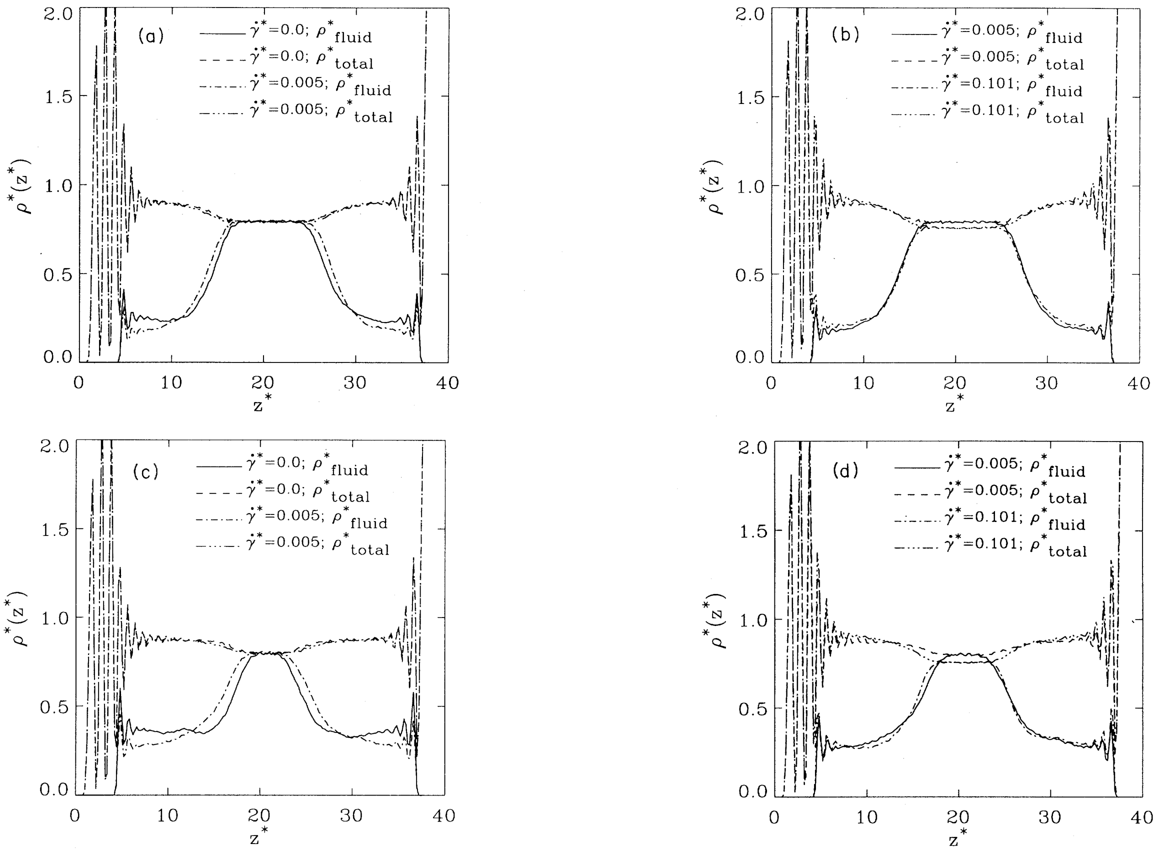

FIG. 5. Density profiles, $\rho^*(z^*)=\rho\sigma^3(z/\sigma)$, computed during the simulation of systems: (a) (LJ+C), (b) (LJ+C), (c) (LJ+SC), and (d) (LJ+SC). Quantities are given in reduced units. See captions for Figs. 2 and 3 for more details.

the width of the density profiles is smaller than the one obtained for the LJ+C system reflecting the stiffness of the chains, which extend further into the fluid region.

Pressure tensor components are shown in Figs. 6 and 7. As for the pure LJ fluid, the normal component is constant across the shear field, but the absolute pressure values are lower, which is due to the configurational contribution from the attractive harmonic potential; see Eqs. (3) and (4). The increase in $P_N(z)$ between the shear rates 0.040 and 0.101 is larger than the one observed for the pure LJ fluid, which is a result of the higher temperature observed in the LJ+C system (see Table I). At low shear rate, the $P_{xz}(z)$ curves for LJ+C are similar to the ones for the LJ fluid. Only at relatively high rates do the profiles differ from those of the pure LJ fluid. The $P_{xz}(z)$ profile of the LJ+C system shows a remarkable increase in the fluid region, whereas for the pure LJ fluid, $P_{xz}(z)$ remains constant across the shear field. As seen from Table I, the temperature evolutions in both systems are significantly different. Higher temperatures and velocity gradients are observed for the LJ+C system, where the latter corresponds to higher shear rates; hence, higher temperature, lower viscosity. As shown by curve (*D*) in Fig. 2, the temperature profile at relatively high shear rates shows a nonparabolic shape. This is an indication that the heat transfer from solvent to wall through the organic layer of amphiphilic molecules is perturbed, and that the solvent and the amphiphilic layer have different thermal conductivities. Although the presence of an amphiphilic layer dramatically changes the heat flow characteristics of the system, the stiffness of the chains has only a small effect on the temperature and velocity gradients.

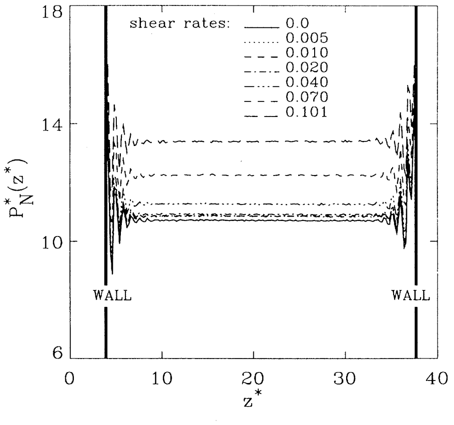

FIG. 6. Normal pressure tensor component profiles, $P^*_N(z^*)$, at different shear rates computed during the simulation of the LJ+C system. Quantities are given in reduced units. See captions for Figs. 2 and 3 for more details.

From the average stress, we are now able to calculate the viscosity profiles using expression (11). As shown in Figs. 8(a)–8(c) the viscosity changes continuously across the slab. The viscosity profiles for the pure LJ fluid [Fig. 8(a)] also show that the signal to noise ratio increases significantly for shear rates smaller than 0.02, and hence, viscosity data cannot be determined with high accuracy. The viscosities of the LJ+C and LJ+SC are a factor of ≈ 2 lower than those of the LJ fluid. This is caused by the much steeper velocity profiles observed in the LJ+C and LJ+SC systems [see insert in Figs. 8(b) and 8(c)]. In both systems, it appears that macroscopically it is as though the wall was moved into the flow a distance corresponding to the hydrodynamic thickness of the layer. This is unexpected for such a low surface coverage of 33%, since the ends of the amphiphilic molecules exposed to the fluid region should be more flexible and could have resulted in a more diffusive interface between the organic layer and the fluid region. In contrast, we observe a relatively sharp interface, which may be caused by the increased solvent density in the chain region close to the interface (see density profiles). Essentially solvent molecules are trapped between the chains reducing the flexibility of the amphiphilic molecules. The increase in $P_{xz}(z)$ is minor compared to the change in the steepness of velocity profiles. Increasing the stiffness of the chains, the viscosity in the fluid regions is only marginally changed reflecting the slightly steeper velocity profiles obtained for the LJ+SC system (see Table I). Compared to the pure LJ fluid and LJ+C system the parabolic function describing $\eta(z)$ becomes narrower with the overall trend: LJ+SC < LJ+C $\ll$ LJ fluid.

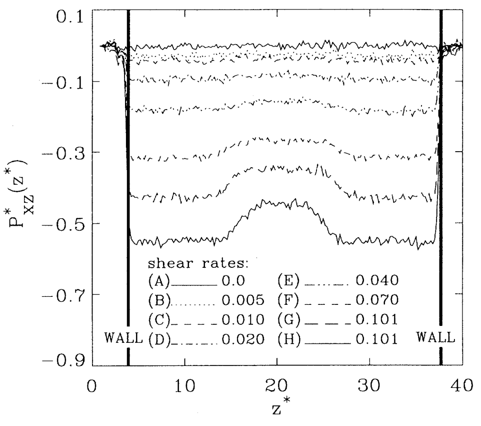

FIG. 7. Off-diagonal pressure tensor component profiles, $P_{xz}^*(z^*)$, at different shear rates computed during the simulations of the LJ+C and LJ+SC systems. Curves (A)–(G) represent the $P_{xz}^*(z^*)$ profiles computed during the simulation of the LJ+C system, whereas (H) was obtained during the simulation of the LJ+SC system. Quantities are given in reduced units. See captions for Figs. 2 and 3 for more details.

In the discussion above, we have qualitatively addressed the structural behavior of the chains which we will now demonstrate more quantitatively. Structural information on the amphiphilic molecules was obtained by computing the mean square radius of gyration and its

TABLE I. Selected thermodynamic data taken at z', where the streaming velocity is zero; $v_x(z')=0$. LJ refers to the purely Lennard-Jones fluid, whereas LJ+C and LJ+SC refer to Lennard-Jones fluid and amphiphilic chains using ($k_{ik}=0\epsilon/\sigma^2$) or ($k_{ik}=30\epsilon/\sigma^2$); see Eqs. (1)–(5).

$\dot{\gamma}^*$	$\frac{dv^*}{dz^*}(z')$	$T^*(z')$	$P_N^*(z')$	$-P_{xz}^*(z')$	$\eta^*(z')$
		LJ model			
0.0	0.0	2.08	13.50	0.0	
0.005	0.005	2.08	13.48	0.009	
0.010	0.011	2.08	13.55	0.015	
0.020	0.020	2.09	13.58	0.039	1.92
0.041	0.039	2.12	13.69	0.076	1.93
0.070	0.072	2.22	14.02	0.135	1.89
0.101	0.109	2.45	14.63	0.182	1.67
		LJ+C model			
0.0	0.0	2.08	10.72	0.0	
0.005	0.020	2.09	10.86	0.021	
0.010	0.039	2.07	10.87	0.047	1.06
0.020	0.073	2.12	10.93	0.086	1.18
0.041	0.144	2.29	11.30	0.156	1.08
0.070	0.253	2.75	12.26	0.271	1.07
0.101	0.363	3.36	13.39	0.346	0.95
		LJ+SC model			
0.0	0.0	2.07	10.89	0.0	
0.005	0.026	2.06	11.06	0.039	1.50
0.010	0.050	2.05	10.98	0.058	1.14
0.020	0.101	2.16	11.19	0.136	1.34
0.041	0.193	2.34	11.58	0.228	1.18
0.070	0.342	2.91	12.58	0.333	0.97
0.101	0.460	3.60	13.84	0.447	0.97

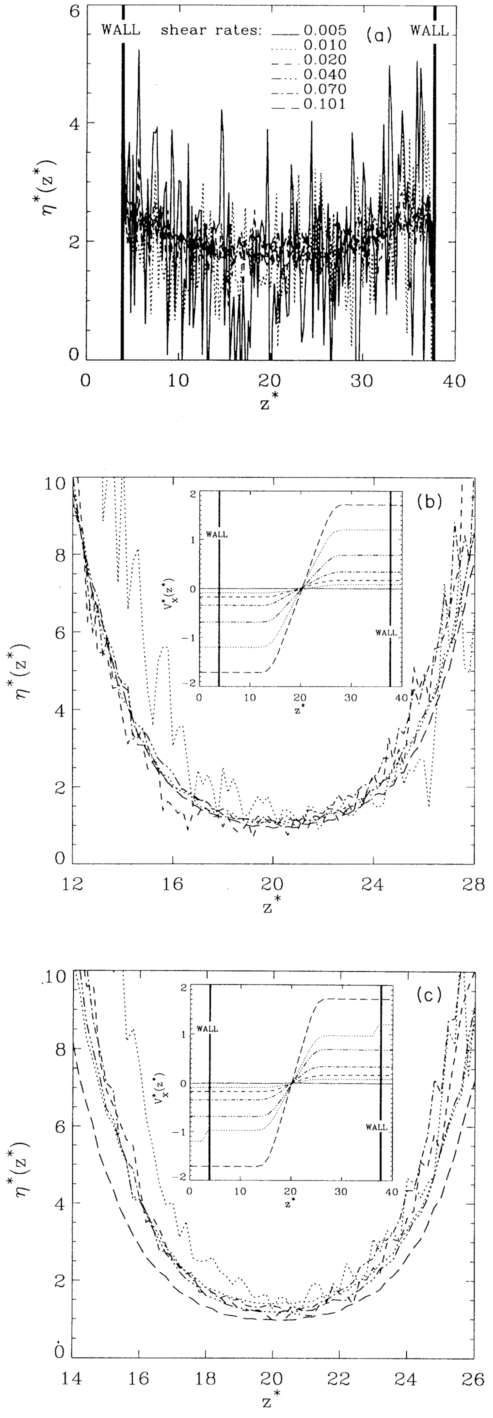

FIG. 8. Viscosity data as a function of shear rate are presented for the following: (a) Lennard-Jones fluid, (b) amphiphilic molecules immersed in solvent (LJ+C). Insert shows the corresponding velocity profiles. Data are given for $\gamma^*(z^*)=0.0$, ——; $\dot{\gamma}^*(z^*)=0.005$, · · · ·; $\dot{\gamma}^*(z^*)=0.010$, — — —; $\dot{\gamma}^*(z^*)=0.020$, —·—·—; $\dot{\gamma}^*(z^*)=0.040$, ···—···—; $\dot{\gamma}^*(z^*)=0.070$, · · · ·; and $\dot{\gamma}^*(z^*)=0.101$, ———. (c) Amphiphilic molecules with stiffer chains immersed in solvent (LJ+SC). Insert shows the corresponding velocity profiles. The different line styles correspond to (b). Quantities are given in reduced units. See captions for Figs. 2 and 3 for more details.

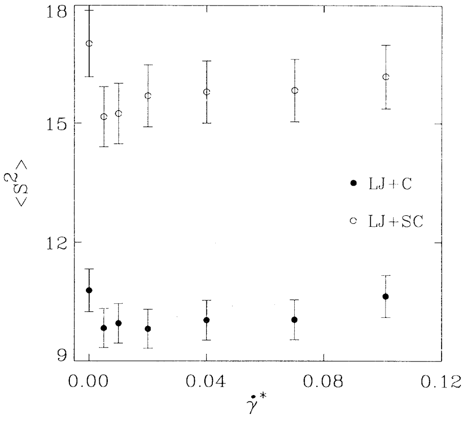

FIG. 9. Mean square radius of gyration of chains determined for the two different model systems LJ+C and LJ+SC. Quantities are given in reduced units. See captions for Figs. 2 and 3 for more details.

components [53,54] as

$$\langle S_{\parallel}^2\rangle=\frac{1}{N}\sum_{k=1}^{N}\langle (x_k-x_{\text{com}})^2+(y_k-y_{\text{com}})^2\rangle \ , \tag{14}$$

$$\langle S_{\perp}^2\rangle=\frac{1}{N}\sum_{k=1}^{N}\langle (z_k-z_{\text{com}})^2\rangle \ , \tag{15}$$

$$\langle S_{\text{tot}}^2\rangle=\langle S_{\parallel}^2\rangle+\langle S_{\perp}^2\rangle \ , \tag{16}$$

where the index "com" refers to the center of mass of each chain. Figures 9, 10, and 11 show the mean-square radius of gyration and its components as a function of shear rate for the two models. Independent of the flexibility of the chains, the amphiphilic molecules respond very sensitively to relative small shear rates. At the lowest shear rate studied, $S_{\perp}^2$ for the LJ+C and LJ+SC systems decreases, which is a result of the depletion of solvent close to the boundary (see density profiles). $S_{\parallel}^2$ increases under shear indicating that molecules are tilted

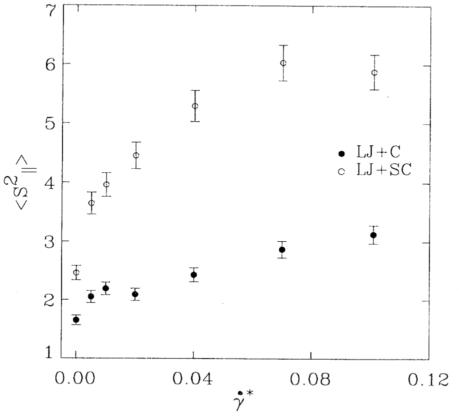

FIG. 10. Mean square radius of gyration parallel to the boundary wall determined for the two different model systems LJ+C and LJ+SC. Quantities are given in reduced units. See captions for Figs. 2 and 3 for more details.

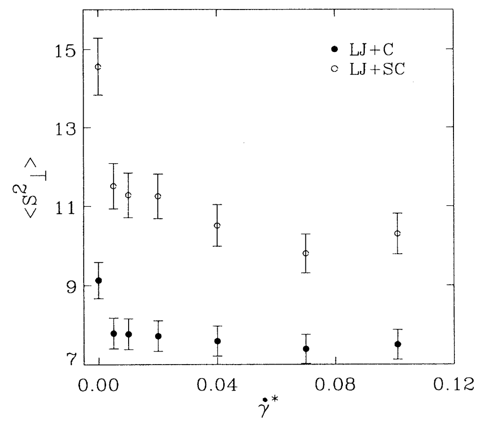

FIG. 11. Mean square radius of gyration perpendicular to the boundary wall determined for the two different model systems LJ + C and LJ + SC.

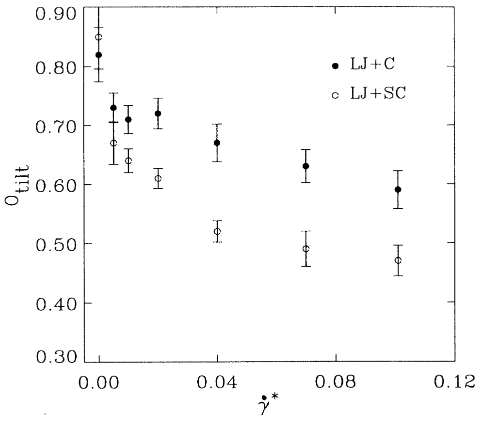

FIG. 12. Tilt order parameter calculated during the simulation of the two different model systems LJ + C and LJ + SC. Quantities are given in reduced units. See captions for Figs. 2 and 3 for more details.

and/or folded. However, $S^2_\perp$ is almost constant for $\dot{\gamma}^* \geq 0.01$, which indicates that the tilt of the amphiphiles is accompanied by a stretching of the chains. The changes observed in $S^2_\parallel$ and $S^2_\perp$ are more significant in the LJ + SC system, where amphiphilic molecules are hindered by an additional harmonic potential described by Eq. (5) to fold in a more compact configuration.

Complementary information about the degree of tilting of the amphiphilic molecules under the influence of shear was deduced from the tilt order parameter O_{tilt} defined in terms of the second Legendre polynomial (P_2):

$$O_{\text{tilt}} = \langle P_2(\cos\theta_i) \rangle = \frac{1}{2N} \left\langle \sum_{i=1}^{N} (3\cos^2\theta_i - 1) \right\rangle . \tag{17}$$

θ_i is the angle between the surface normal, $\hat{z}$, of the boundary (see Fig. 1) and the long axis of molecule i, which is defined as that eigenvalue of the inertia moment tensor with the smallest eigenvector. The tilt order parameters as a function of shear rates are shown in Fig. 12. Increasing the stiffness of the amphiphilic molecules yields a larger tilt. The molecules can only escape from the induced shear stress by tilting, whereas a more flexible molecule has an additional degree of freedom in folding, which would also be reflected in a decrease in $S^2_\perp$.

IV. CONCLUSION

We have performed nonequilibrium molecular dynamics simulations to measure the viscosity profiles of fluids in narrow walls coated with amphiphiles. The physical properties of this complex system are defined by a large number of parameters, i.e., wall separation, chain length, chain stiffness, surface coverage, shearing velocity, etc. We have focused on a small set of parameters, which is feasible to simulate and sufficient to gain a basic understanding of the rheology of this model system. We have chosen a low surface coverage to examine the interplay between solvent and amphiphiles at a range of reduced shear rates varying from 0.0 to 0.101. The lowest shear rate of 0.005 considered in this study presents a threshold, where below that value no reliable stress and viscosity data could be computed.

The most interesting result is that the chains behave like a wall, which is reflected in the steep velocity profiles and in the remarkable changes in the mean square radius of gyration. $S^2_\perp$ already drops significantly at low shear rate and does not change with increasing shear rates, whereas $S^2_\parallel$ increases continuously with increasing rate. An indication that the tilt of the amphiphilic molecules due to the shear induced flow is accompanied by an elongation of the chains. Increasing the stiffness of the chains yields a significant change in the geometrical quantities, but only affects the flow behavior slightly. At low shear rate, the stress ($-P_{xz}$) is constant across the slab, and can directly be computed at the wall. Only at higher shear rates, the stress is influenced by the temperature and is no longer constant across the shear field. The temperature profiles become increasingly nonparabolic, indicating that the fluid and layer of amphiphiles have a different thermal conductivity. This effect is more pronounced for less flexible chains.

ACKNOWLEDGMENTS

Computations were performed at the University of Southampton, University of Copenhagen (Grant No. SNF 11-0065-1), and at Novo-Nordisk A/S. G.H.P. would like to acknowledge financial support from the European Grants No. CHRX CT 930092/190 and No. BIOZ-CT93-5507. D.J.T. would like to thank the EPSRC for Grant No. GR/J/74459 for computing equipment.

[1] H. Yoshizawa, Y.-L. Chen, and J. Israelachvili, J. Phys. Chem. **97**, 4128 (1993).

[2] H. Yoshizawa and J. Israelachvili, J. Phys. Chem. **97**, 11 300 (1993).

[3] P. A. Thompson and M. O. Robbins, Science **250**, 792 (1990).

[4] V. Schmitt, F. Lequeux, A. Pousse, and Roux, Langmuir **10**, 955 (1994).

[5] M. L. Gee, P. M. Mcguiggan, J. Israelachvili, and A. M. Homola, J. Chem. Phys. **93**, 1895 (1990).

[6] R. G. Horn, S. J. Hirz, G. Hadzlioannou, C. W. Frank, and J. M. Catala, J. Chem. Phys. **90**, 6767 (1989).

[7] J. Van Alsten and S. Granick, Phys. Rev. Lett. **61**, 2570 (1991).

[8] H.-W. Hu and S. Granick, Science **258**, 1339 (1992).

[9] G. M. McLelland, *Adhesion and Friction* (Springer, Berlin, 1989).

[10] S. Sharma and L. V. Woodcock, J. Chem. Soc. Faraday Trans. **87**, 2023 (1991).

[11] B. N. J. Persson, Phys. Rev. Lett. **71**, 1212 (1993).

[12] P. A. Thompson and M. O. Robbins, Phys. Rev. A **41**, 6830 (1990).

[13] S. Y. Liem, D. Brown, and J. H. R. Clarke, Phys. Rev. A **45**, 3706 (1992).

[14] Y. Liem, Ph.D. thesis, University of Manchester, 1992.

[15] T. K. Xia, J. Ouyang, M. W. Ribarsky, and U. Landman, Phys. Rev. Lett. **69**, 1967 (1992).

[16] P. Padilla and S. Toxvaerd, J. Chem. Phys. **101**, 1490 (1994).

[17] J. B. Sokoloff, Phys. Rev. B **42**, 760 (1990).

[18] W. Zhong and D. Tomanek, Phys. Rev. Lett. **64**, 3054 (1990).

[19] J. A. Harrison, C. T. White, R. J. Colton, and D. Brenner, Phys. Rev. B **46**, 9700 (1992).

[20] J. A. Harrison, C. T. White, R. J. Colton, and D. Brenner, J. Phys. Chem. **97**, 6573 (1993).

[21] J. N. Glosli and G. M. McClelland, Phys. Rev. Lett. **70**, 1960 (1993).

[22] Y. H. Kim, J. T. Nelson, and B. Glynn, Cereal Foods World **39**, 8 (1994).

[23] P. G. Gennes, Macromolecules **13**, 1069 (1980).

[24] P. G. Gennes, *Scaling Concepts in Polymer Physics* (Cornell University Press, Ithaca, NY, 1979).

[25] A. Baumgärtner, *Application of the Monte Carlo Method in Statistical Physics,* edited by K. Binder (Springer, Berlin, 1984).

[26] K. Binder, *Computational Modeling of Polymers* (J. Biorano, New York, 1992).

[27] M. Murat and G. S. Grest, in *Computer Simulations of Polymers,* edited by R. J. Roe (Prentice-Hall, Englewood Cliffs, NJ, 1991).

[28] K. Binder, *Monte Carlo Methods in Statistical Physics* (Springer, Berlin, 1979).

[29] D. J. Diestler, M. Schoen, and J. H. Cushman, Science **262**, 545 (1993).

[30] J. Atkinson, C. J. Goh, and N. Phan-Thien, J. Chem. Phys. **80**, 6305 (1984).

[31] P.-Y. Lai and K. Binder, J. Chem. Phys. **98**, 2366 (1993).

[32] G. S. Grest and K. Kremer, Phys. Rev. A **33**, 3628 (1986).

[33] K. Kremer and G. S. Grest, J. Chem. Phys. **92**, 5057 (1990).

[34] K. Kremer and G. S. Grest, in *Computer Simulations of Polymers* (Ref. [27]).

[35] K. Kremer, *Computer Simulation in Chemical Physics,* Vol. 397 of *NATO Advanced Study Institute, Series C: Mathematical and Physical Science,* edited by M. P. Allen and D. J. Tildesley (Kluwer Academic, London, 1993).

[36] M. Murat and G. S. Grest, Phys. Rev. Lett. **63**, 1074 (1989).

[37] K. J. Chugg, Ph.D. thesis, St. Edmunds College, Cambridge, U.K., 1990.

[38] J. D. Weeks, D. Chandler, and H. C. Andersen, J. Chem. Phys. **54**, 5237 (1971).

[39] M. P. Allen and D. J. Tildesley, *Computer Simulation of Liquids* (Clarendon, Oxford, 1989).

[40] W. G. Hoover, *Molecular Dynamics* (Springer, Berlin, 1987).

[41] D. J. Evans and G. P. Morriss, *Statistical Mechanics of Non-Equilibrium Liquids* (Academic, London, 1990).

[42] S. Toxvaerd, Mol. Phys. **72**, 159 (1991).

[43] W. G. Hoover, Phys. Rev. A **31**, 1695 (1985).

[44] W. T. Ashurst and W. G. Hoover, Phys. Rev. A **11**, 658 (1975).

[45] W. G. Hoover, D. J. Evans, R. B. Hickman, A. J. C. Ladd, W. T. Ashurst, and B. Moran, Phys. Rev. A **22**, 1690 (1980).

[46] D. J. Evans and G. P. Morriss, Phys. Rev. A **30**, 1528 (1984).

[47] A. J. C. Ladd, Mol. Phys. **53**, 459 (1984).

[48] H. A. Barnes, J. F. Hutton, and K. Walters, *An Introduction to Rheology* (Elsevier, Amsterdam, 1989).

[49] J. P. R. B. Walton, D. J. Tildesley, and J. S. Rowlinson, Mol. Phys. **48**, 1357 (1983).

[50] J. P. R. B. Walton, D. J. Tildesley, and J. S. Rowlinson, Mol. Phys. **58**, 1013 (1986) (erratum).

[51] D. H. Tsai, J. Chem. Phys. **70**, 1375 (1979).

[52] J. S. Rowlinson and B. Widom, *Molecular Theory of Capillarity* (Clarendon, Oxford, 1989).

[53] P. J. Flory, *Statistical Mechanics of Chain Molecules* (Interscience, New York, 1986).

[54] M. Doi and S. F. Edwards, *The Theory of Polymer Dynamics* (Clarendon, Oxford, 1986).